

RESEARCH ARTICLE

Metal Cutting Data Integration with Different Contact and Friction Conditions, Kinematics, Tool Geometry, and Temperatures

Wolfgang Lortz^{1,*}

¹*Mechanical Department, University of Applied Sciences, Germany*

Abstract: The data integration with additional artificial intelligence (AI) creates a lot of interest in industry as well as in the scientific world. The aim is to determine the complete production result before processing. But before we develop the complicated mathematical algorithm for creating a relevant digital machining process, the true nature of the process must be understood. A systematic analysis of the existing metal machining process reveals several different problem areas with an interdependent relationship. There is a metal deformation process that depends on the existing material properties influenced by stress, strain rate, hydrostatic pressure, and temperature. This problem area will be mathematically described and result in adequate equations for the stress and strain-rate situation for developing the existing plastic deformation. The next problem area is determined by the physical relation of contact and friction around the tool. Why do built-up edge, built-up layer, and material flow blockade occur at the tool, and what are the consequences of all these phenomena on the cutting process? Furthermore, where does the dynamic process come from, accompanied by dynamic forces and resulting in different temperatures and discontinuous chip flow? All this will be discussed in this paper and presented with practical evidence.

Keywords: metal cutting data -integration, contact and friction condition, cutting velocity and tool geometry

1. Introduction

In recent years, many attempts have been made to gain a better understanding of the complex nature of the metal cutting process, but there are still some gaps in our knowledge regarding the chip formation process characterized by high plastic deformation with volume conservation and material movement along special deformation lines creating self-hardening or temperature effects. Furthermore, the contact and friction conditions in the interface tool material are changing progressively due to the velocity and the geometric dimensions of the tool. All these phenomena create different dynamic behavior resulting in body forces with an influence on the whole machining process.

Thus, the aim of this work is an analytical description of the dynamic cutting process, taking into account the following aspects:

- Material properties
- Mathematical development of stress and strain
- Contact and friction conditions
- Physical interpretation of the developed equations describing plasticity during cutting
- The influence of cutting velocity
- The influence of tool geometry on plastic deformation during machining
- Development of the created temperature

- Development of the influenced subsurface

All these phenomena will be compared with practical results.

2. Literature Review

The previous models in metal cutting make a lot of assumptions for simplifying the model. Take the pioneer work of Merchant [1] straight shear line model. Many years ago, Shaw [2] mentioned that there was a lot of interest in this model, but despite countless attempts, the real solution has never been found.

For more than 40 years, scientists [3–5] have leveraged the computer for solving technological problems by finite element modeling. In the beginning, there was considerable interest with a lot of enthusiasm in this model. But until today, agreement with practical results is still missing.

Due to this fact, scientists used high-speed cameras for monitoring the chip formation process [6, 7], but the stress and temperature situation at the surface is quite different from the distribution inside the material, and in addition, there is a chip side flow [8] – what are they really measuring?

The knowledge of the contact and friction condition in the interface between the chip and tool provides a very important step to a complete cutting model [9]. The temperatures in the contacting zone were simulated and presented by Meurer et al. [10]. But unfortunately, the real material behavior (all metals and their alloys can deform only on special gliding lines, as well as the existing contact conditions) was ignored, so the result was very questionable.

***Corresponding author:** Wolfgang Lortz, Mechanical Department, University of Applied Sciences, Germany. Email: wllr3085@hochschule-trier.de, woma-lortz@outlook.com

An important contribution to the machining process is the residual stresses, concerning the microstructure of the material as well as the deformed layers in the workpiece subsurface [11–14]. But agreement between modeled and experimental results is still missing.

That is the reason scientists are searching for an alternative. Some are focused more on practical measurements. Saelzer et al. [15] built a test setup for measuring the temperatures in the contacting area. But what do they really measure if there is a built-up edge (BUE), a built-up layer (BUL), or diffusion at the tool surface?

Until today, the contact and friction conditions in the interface between tool and chip are unknown [16]. That might be the reason why some scientists [17, 18] start with the Coulomb friction law ($\mu = F_t/F_n$). But this friction law was developed for friction between two rigid, solid bodies without any plasticity in the contacting zone. Based on this fact, some scientists [19, 20] changed the strategy – a pin was pressed into a rotating disk, and friction was defined as $\mu = F_t/F_n$, and they called this setup “tribometer,” but what do they really measure? – A plowing process with corresponding material transport.

The development of the complete metal cutting process, as a base for artificial intelligence (AI) with high degree of conformity between experimental and analytical results, is much more complicated.

2.1. Theoretical framework

Due to the vague assumptions, all the mathematical equations for describing the cutting process are far from reality. The mathematical development of adequate equations for solving the dynamic cutting process is much more difficult – as we will see in this chapter. But let the critical reader of this paper form his or her own opinion.

The mathematical development for stress:

At a given point in the plastic area, the state of stress can be formulated by the stress deviator in addition to the interference factor “dynamic body forces” as follows:

$$\begin{pmatrix} \sigma_x - \sigma_m & \tau_{xy} & \tau_{xz} \\ \tau_{yx} & \sigma_y - \sigma_m & \tau_{yz} \\ \tau_{zx} & \tau_{zy} & \sigma_z - \sigma_m \end{pmatrix} \pm \text{dyn. part} = 0 \quad (1)$$

With $\sigma_m = \frac{1}{3}(\sigma_1 + \sigma_2 + \sigma_3) = p$ (hydrostatic pressure)

For two dimensions with $z = 0$, it follows:

$$\begin{pmatrix} \sigma_x - \sigma_m & \tau_{xy} \\ \tau_{yx} & \sigma_y - \sigma_m \end{pmatrix} \pm \text{dyn. part} = 0 \quad (2)$$

For the static part, we can write

$$(\sigma_x - \sigma_m)(\sigma_y - \sigma_m) + (\tau_{xy})^2 = \text{circle} \quad (3)$$

and with

$$\sigma_m = \frac{1}{2}(\sigma_x + \sigma_y) \quad \text{we get:} \quad (4)$$

$$\left(\sigma_x - \frac{1}{2}(\sigma_x + \sigma_y)\right)\left(\sigma_y - \frac{1}{2}(\sigma_x + \sigma_y)\right) + (\tau_{xy})^2 = (k_f)^2 \quad (5)$$

Or

$$\left(\frac{\sigma_y - \sigma_x}{2}\right)^2 + (\tau_{xy})^2 = (k_f)^2 \quad (6)$$

This equation represents a circle with the radius k_f , better known as Mohr's circle for stress.

The dynamic part represents the acceleration of $a(t)$ particles due to body forces – depending on time and space – and can be formulated as:

$$a(t) = -\Delta v \frac{1}{t^*} + v_0 \omega \frac{1}{t^*} \cos \omega \frac{t}{t^*} \quad (7)$$

Taking the equation for stress (2) and substituting the values σ_x , σ_y , and τ_{xy} from Mohr's circle, we can obtain two nonlinear partial differential equations.

Substituting ∂x with ∂s_1 and ∂y with ∂s_2 leads finally to the following integral:

$$-p - \int \frac{\partial p}{\partial s_2} ds_1 - 2k\phi - \int \frac{\partial k}{\partial s_2} ds_1 \pm a_{s_1} \rho ds_1 = c \quad (8)$$

$$-p - \int \frac{\partial p}{\partial s_1} ds_2 + 2k\phi + \int \frac{\partial k}{\partial s_1} ds_2 \mp a_{s_2} \rho ds_2 = c \quad (9)$$

The final result for the stress situation is characterized by the following influencing factors:

- Hydrostatic pressure p
- Self-hardening increase in hydrostatic pressure
- Yield shear stress k_f
- Influence of self-hardening on yield shear stress
- Body forces written as stress
- Resultant value in the plastic area

The mathematical description of the strain-rate criterion in plane strain is similar to the already developed yield shear stress state.

The state of strain rate can be described by the following strain-rate deviator:

$$\begin{pmatrix} \frac{\partial v_x}{\partial x} & \dot{\varepsilon}_{xy} & \dot{\varepsilon}_{xz} \\ \dot{\varepsilon}_{yx} & \frac{\partial v_y}{\partial y} & \dot{\varepsilon}_{yz} \\ \dot{\varepsilon}_{zx} & \dot{\varepsilon}_{zy} & \frac{\partial v_z}{\partial z} \end{pmatrix} \pm \text{dyn. part} = 0 \quad (10)$$

For two dimensions with $\dot{\varepsilon}_z = 0$, it follows:

$$\begin{pmatrix} \frac{\partial v_x}{\partial x} & \dot{\varepsilon}_{xy} \\ \dot{\varepsilon}_{yx} & \frac{\partial v_y}{\partial y} \end{pmatrix} \pm \text{dyn. part} = 0 \quad (11)$$

And from equation (11), it can be obtained:

$$-\dot{\varepsilon}_x \dot{\varepsilon}_y + (\dot{\varepsilon}_{xy})^2 \pm a dt = 0 \quad (12)$$

From volume conservation, it follows:

$$\dot{\varepsilon}_y = -\dot{\varepsilon}_x \quad (13)$$

The result of equations (12) and (13) can be written as:

$$(\dot{\varepsilon}_x)^2 + (\dot{\varepsilon}_{xy})^2 \pm a \, dt = 0 \quad (14)$$

The first part represents a centric circle with the radius $\dot{\varepsilon}_0$.

Better known as Mohr's circle for strain rate. The second part represents the strain-rate discontinuity, responsible for additional body forces.

Taking the equation for strain rate (11) and substituting the values for $\dot{\varepsilon}_x$, $\dot{\varepsilon}_y$, and $\dot{\varepsilon}_{xy}$ from Mohr's circle and applying a total differentiation lead to the final equation:

$$\dot{\varepsilon}_0 \int \left(\frac{\partial \phi}{\partial s_1} - \frac{\partial \phi}{\partial s_2} \right) ds_1 \mp a_{s_1} \, dt = v_{res} \quad (15)$$

$$-\dot{\varepsilon}_0 \int \left(\frac{\partial \phi}{\partial s_2} - \frac{\partial \phi}{\partial s_1} \right) ds_2 \mp a_{s_2} \, dt = v_{res} \quad (16)$$

The final result for the state of strain rate is characterized by the following vectors:

- The first vector represents the cutting velocity v_c .
- The second vector represents the self-hardening effect v_{sh} .
- The third vector represents the strain-rate discontinuity v_{dyn} .
- The fourth vector represents the resultant vector v_{res} .

In the next step, it will be shown that from the knowledge of the resultant vector, the deformation of a particle can be developed.

From physics, we know that $v = ds/dt$: taking $dt = \text{const.}$, it follows:

$$v \sim ds \quad (17)$$

These systematically developed equations for yield shear stress (8) as well as strain rate (15), together with the acceleration $a(t)$ (7),

are the mathematical-physical fundamentals for developing the grid deformation "ds" during metal plastic flow.

These new developed mathematic and physic equations are right or wrong and can't not be quantitative validated. For proofing the correctness of these developed equations, practical tests with different cutting conditions and different tool geometry were taken and are presented in this paper.

3. Research Methodology

3.1. Material properties

All metal and their alloys can deform plastically only on special gliding lines (see left-hand side of Figure 1). These gliding lines have an orthogonal relationship and represent the maximum shear stress τ_{max} . Next to this, the hydrostatic pressure p has a high impact on the plasticity of the body. Practical tests have shown that the hydrostatic pressure alone does not cause material to flow. The flow of the material is initiated by the difference between stress σ and the hydrostatic pressure p (see right-hand side of Figure 1).

3.2. Material behavior influenced by self-hardening and temperature

The material behavior yield shear stress versus deformation is known. With increasing deformation, a self-hardening effect can be recognized. But some former publications ignored this effect, and their calculation was based only on "ideal plastic behavior" (see left-hand side of Figure 2). During the cutting operation, we start with self-hardening at the first plastic boundary line "A" until the deformation increases to a special value, and from that point, temperature becomes dominant.

Figure 1
Tensile and compression test with plastic deformation influenced by hydrostatic pressure p

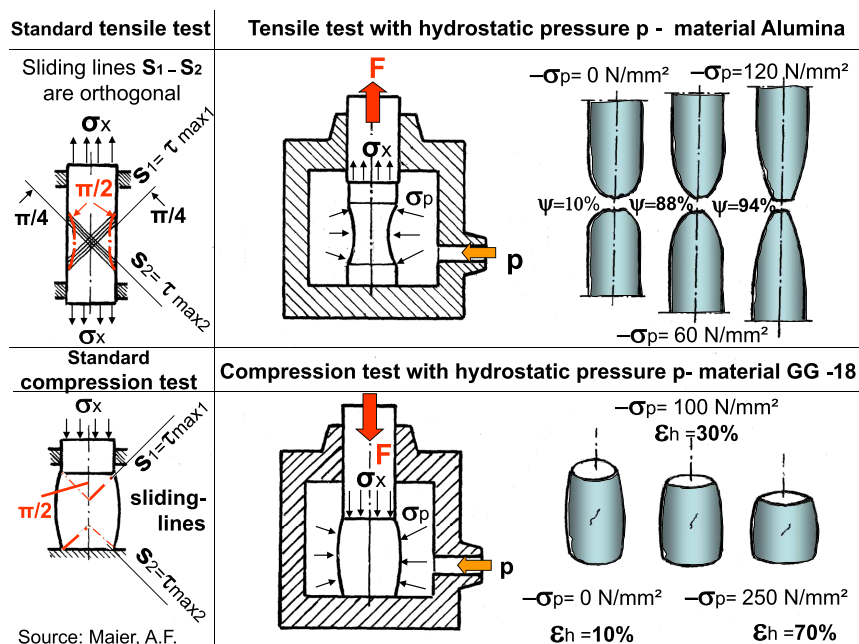


Figure 2

Average values of yield shear stress versus natural strain and temperatures – interdependent behavior of strain versus temperatures

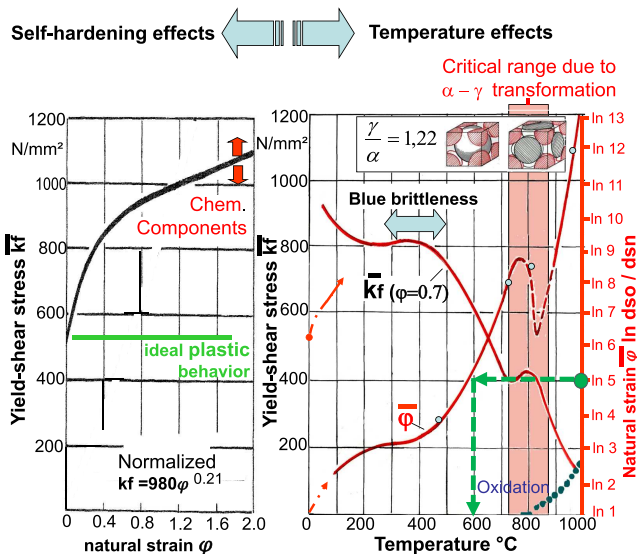
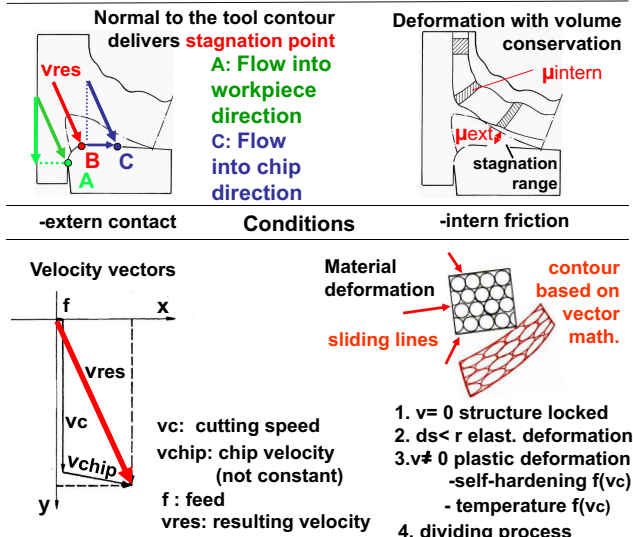


Figure 3

Contact and friction conditions during metal plastic flow

Friction in metal plasticity

Complex contact and friction conditions during metal plastic flow



The material behavior yield shear stress versus temperatures is known and documented on the right-hand side of Figure 2. Due to temperature influence, the yield shear stress will decrease. Due to interdependent relationships between stress and natural strain, the deformation will increase. Thus, as long as we know the deformation of the material, we can estimate the existing temperature.

3.3. Contact and friction conditions during metal plastic flow

The contact and friction conditions are determined by the existing velocities at the tool contour. The cutting velocity v_c and the

chip velocity v_{chip} result in a vector v_{res} . At one point, this resulting vector will meet the tool contour in a normal direction. This delivers a stagnation point (see the red arrow v_{res} in Figure 3). Due to the fact that all metals, as well as their alloys, have a crystalline structure and can deform only on special gliding lines, a stagnation area will be created, and the plastic material will flow along these gliding lines with friction.

Thus, we have to consider two phenomena: first, the contact creates a stagnation area, and second, the friction at the stagnation border line.

This contact state creates a BUE. Due to the dynamic chip flow, the top of the hardened BUE will move to the “left,” and the other part will move to the “right.” The movement to the left creates a squeezing effect, and this squeezing will create high temperatures with a bad subsurface and high flank wear.

If the cutting velocity increases, the dead zone develops into a doughy state in plasticity, which will be called a built-up layer BUL.

But what will happen if the metal inflow angle to the tool changes more in vertical position due to lower chip velocity? A chip flow blockade will be created.

Friction at the border range of BUE occurs if the external forces deform the crystalline metal structure at first elastically and then plastically. For this case, the externally applied stress must overcome the internal bonding forces of the crystallites. For this reason, we can discuss four different cases (see right-hand side of Figure 3):

- 1) As long as the velocity is zero, the structure is locked.
- 2) As long as the deformation is smaller than the grain radius r , there occurs only elastic deformation (very small in relation to plastic deformation).
- 3) Increasing velocity with greater deformation results in a .
 - Self-hardening effect or in a
 - Temperature effect
- 4) For extremely high deformation, a dividing process will follow.

On the one hand, this might be very logical, but on the other hand, it is very complex and difficult to implement these phenomena into the metal cutting process. This will be shown and discussed in the next chapter.

3.4. The cutting process with different velocities and tool geometry

Figure 4 presents the cutting forces versus the cutting velocity v_c measured with a “Kistler dynamometer.” The fact is that all cutting forces exhibit dynamic behavior. But the question arises: “Where does the dynamic come from?”

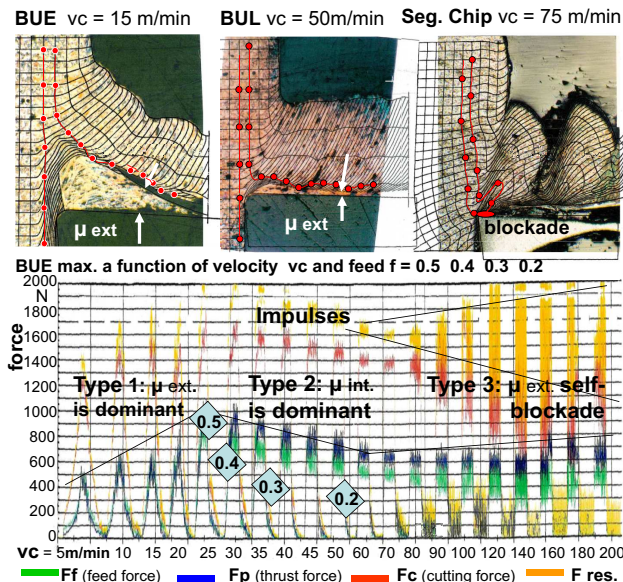
In the low-speed range, a “built-up edge” (BUE) with high material hardening occurs. The maximum BUE is at a feed rate of $f = 0.5$ mm/rev. at $v_c = 20$ m/min. The position of this maximum is not constant, but shifts with lower feed rates ($f = 0.4; 0.3; 0.2$ mm/rev) to higher cutting speeds v_c , whereby the dynamic character is retained (see Figure 4).

In the upper part of Figure 4, you can see three different cross-sections created from a “quick stop” with a theoretically developed grid deformation pattern and “streamlines.” These streamlines flow in the direction of the tool and are divided at the tip of the BUE.

If the cutting speed v_c is increased, the BUE develops into a BUL (built-up layer) as a result of higher temperatures in the

Figure 4

Measured dynamic forces versus cutting velocity (Kistler dynamometer) compared with different deformation zones due to contact and friction conditions



interface chip tool (see Figure 15, more than 700°C). The stream lines are separated by the BUL and float on a “doughy bubble.”

If the cutting speed v_c is increasing further, the material flow at the tip of the tool will lead to a self-blocking effect due to the low chip flow velocity. This self-blocking initially leads to a bulge, and as the process progresses, a chip forms within the deformed bulge and leads to a segmented chip.

The resulting chip rotates and shifts “upwards.” This overcomes the self-blocking effect, and the flowing chip falls onto the tool contour, creating an impulse (see Figure 4 in yellow color) and at the same time generating crater wear.

All these phenomena will be theoretically developed and discussed in the following section.

3.5. Simulation and modeling of the cutting process – based on the developed equations for stress and strain rate – compared with practical results

The derived equations (7), (8), and (15) can be used to adequately determine the deformations during the machining process.

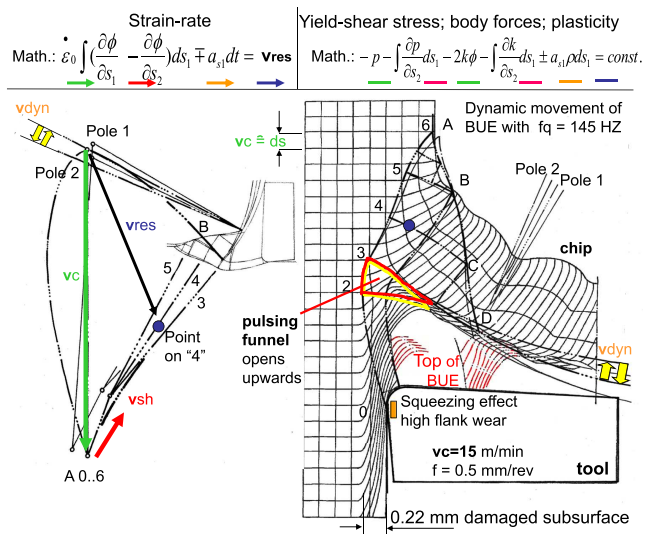
In Mohr's circles for stress and strain rate, the corresponding values are opposite. That means in the physical plane, they are orthogonal.

Thus, the total stress plane and the corresponding strain-rate plane are orthogonal in the physical plane (see Figure 5) and have an interdependent relationship.

The mathematical equation for the stress plane shows that the deformations in the stress plane are determined by the yield stress k as well as by the hydrostatic pressure p . Both values are not constant but change along the “gliding lines,” thus creating a plastic deformation, which, depending on the degree of deformation, leads to a self-hardening or a temperature effect. In addition, a dynamic effect will be created by the opening of a singularity. This opening

Figure 5

The dynamic cutting conditions under BUE creating grid deformation with volume conservation



singularity develops a strain-rate discontinuity, and this strain-rate discontinuity creates an acceleration “ a ” (see equation (7)), and this phenomenon creates, according to Newton’s axiom, $F = m a(t)$, an additional body force. These dynamic body forces create additional deformation of the plastic zone.

First of all, the relevant mathematics for strain rate, as well as for yield shear stress, is presented in the upper part of Figure 5.

- The green vector represents the cutting velocity v_c .
- The red vector represents the velocity as a result of the self-hardening effect v_{sh} .
- The yellow vector represents the periodical change of velocity as a result of body forces v_{dyn} .
- Together, they create the resultant velocity v_{res} in blue.

This resultant vector *vres* is responsible for the deformation *ds* in the stress plane. Making an example, at a certain point “4” (indicated in blue in the strain-rate area as well as in the yield shear stress area), *vres* is given as a vector in the strain-rate area. With a multiplication of $C = 0.051$, we get the deformation value “*ds*” in the yield shear stress plane as well as the corresponding direction in point “4.” From physics, we know that $v = ds/dt$ – for *dt* constant, we get:

$ds \equiv v dt$ or $ds \equiv Cv$ or $v \approx ds$

In Figure 5, this value “C” is 0.051.

But before we can estimate the deformation ds in the yield shear stress area, the total stress plane must be developed.

For the determination of the stress plane, the boundary line "A" must be found. This "A" line starts at the surface at point A6 at 45° (τ_{\max}) with a tension of k and a hydrostatic pressure of k . The contour of this "A" line is primarily determined by the hydrostatic pressure p (in point A5, $p = 1.66 \text{ k}$; in A4, $p = 1.56 \text{ k}$; in A3, $p = 1.44 \text{ k}$).

The points A6–A3 and D defined the first plastic deformation plane.

There exists another second plane characterized by the contact and friction conditions Ao, A2, and D.

These two planes generate a third plane – a triangle A3, A2, C3 – with a singularity in C3 (indicated in yellow color). This singularity must open so that the inflowing material can leave the triangle in point C3 (indicated in red color), and this effect creates a velocity discontinuity with additional body forces. Thus, the total cutting area is characterized by three different but interdependent relationships.

Furthermore, this additional acceleration changes the material flow at the top of the BUE (see Figure 5), and as a result, the hardened particles of the BUE move pulsating to the left-hand

and right-hand side, creating a high mechanical deformation of the workpiece subsurface and a high flank wear on the tool.

The frequency can be estimated by $f_q = 145$ HZ, and the depth of damaged subsurface delivers a value of 0.22 mm. In addition, this pulsing effect is demonstrated in the stress plane as well as in the strain-rate plane, as the difference between Pole 1 and Pole 2 is indicated as v_{dyn} .

Figure 6 demonstrates the comparison between the practical and theoretical results, and I hope that the reader of this paper will agree that this is a good agreement.

For a higher speed of $v_c = 50$ m/min, the velocity and stress plane will change together with the contact and friction conditions.

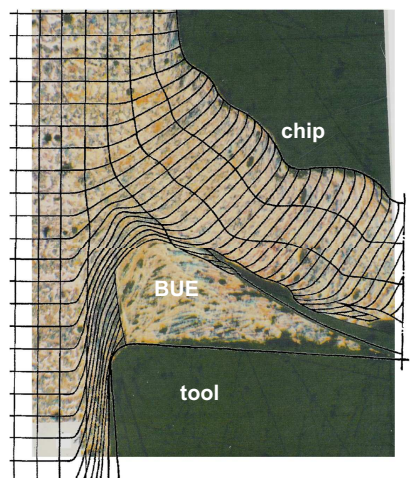
The first boundary "A" line started at an angle of 45° with a yield shear stress of k and a hydrostatic pressure $p = k$. Along the "A" line, the following hydrostatic pressures occur at the points (A5 $p = 1.63$ k; A4 $p = 1.95$ k; A3 $p = 1.8$ k), while the yield shear stress k remains constant. In addition, the contact and friction conditions are changing. At a temperature of 700° C, the BUE degenerates into a BUL. On the one hand, this phenomenon reduces the mechanical influence on the workpiece subsurface, and on the other hand, the crater wear at the tool will be influenced. But the crater wear will never start at the tip of the tool.

The pulsating triangle, or if you like funnel, will also change. Due to the low strength of the BUL, the singularity opens downward (see the yellow and red triangles in Figure 7) and shifts the entire stress plane into this direction. In the strain-rate plane, this dynamic process can be represented by the difference between the two poles, 1 and 2 ($v_{dyn} = \text{Pole1} - \text{Pole2}$).

This theoretical result can be compared with a cross-section of this region. Once again, a good agreement could be achieved (see Figure 8).

A further increase in the cutting speed to $v_c = 75$ m/min changes the contact and friction conditions considerably. The material flow in the interface between the material and the tip of the tool leads to chip flow blockage, and this blockage creates, in a first step, a deformed bulk.

Figure 6
Comparison between the theoretically developed grid deformation and the experimental result



$v_c = 15$ m/min, $f = 0.5$ mm/rev., pos. rake angle, material C45

Figure 7
The cutting result under BUL (built-up layer)

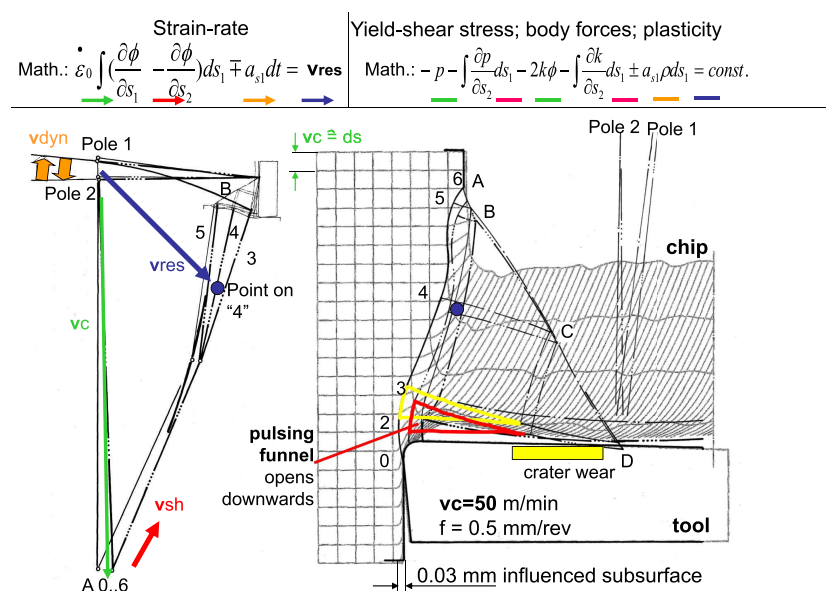
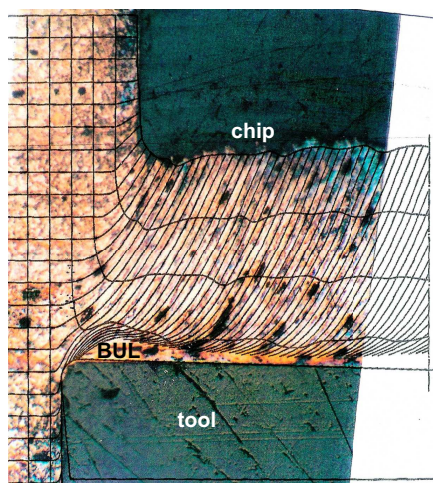
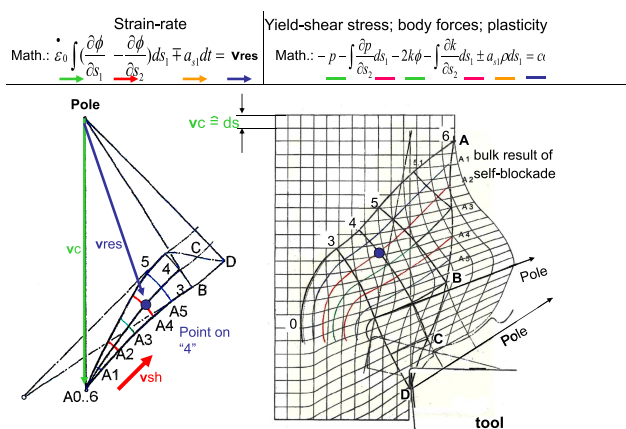


Figure 8
Comparison between the theoretically developed and the experimental result



$v_c = 50 \text{ m/min}$, $f = 0.5 \text{ mm/rev.}$, pos. rake angle, material C45

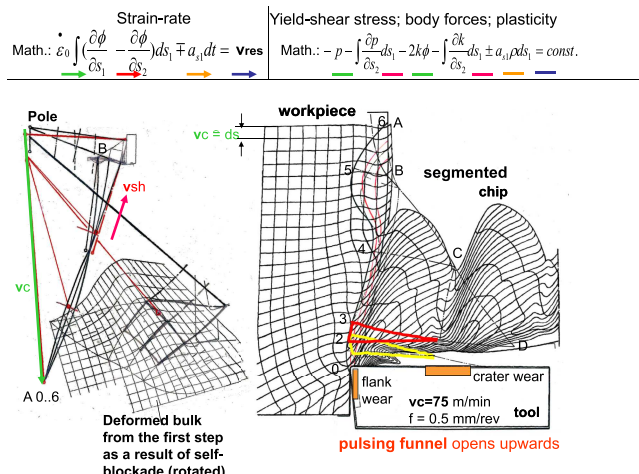
Figure 9
Cutting conditions under self-blockade – first, a bulk with volume conservation will be created



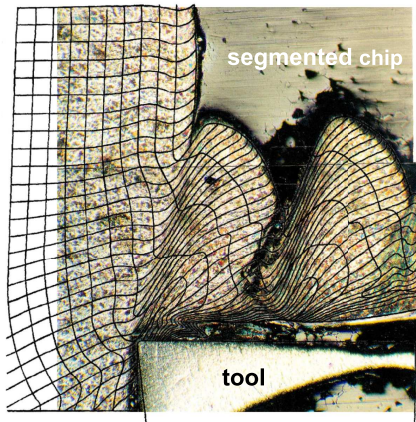
The resulting stress and strain-rate planes are shown in Figure 9. The first boundary line "A" starts at the surface in point A6 at an angle of 45° and with a hydrostatic pressure of $p = k$. At the "A" line, the yield shear stress is constant (first deformation line k). The change of p on the "A" line is responsible for the contour of the line as well as the total stress plane, including plastic deformation. The variation of p could be calculated as follows: In A5, $p = 1.52 \text{ k}$; in A4, $p = 1.28 \text{ k}$; in A3, $p = 1.05 \text{ k}$; and in A0, $p = 2.96 \text{ k}$. This determined stress plane, together with the corresponding strain-rate plane, provides the deformation of the bulk.

In a second step, an additional deformation structure will follow. The newly developed stress field – together with the inter-dependent strain-rate situation – leads to a deformation of the bulk, and as a result of that, a segmented chip will follow (see Figure 10). The chip flow can start when the singularity C23 opens upward, and the stress field rotates and frees the chip from the self-blockade with a frequency of $f_q = 500 \text{ Hz}$.

Figure 10
The cutting conditions under self-blockade create, in a first step, a deformed bulk (presented in the strain-rate area) and with an increasing stress situation, in a second step, a segmented chip, and with an opening of the singularity upward, the chip segment can flow



Figures 11
Comparison between practical and theoretical result



$v_c = 75 \text{ m/min}$, $f = 0.5 \text{ mm/rev.}$, pos. rake angle, material C45

The next Figure 11 presents evidence between the practical and theoretical results. From my point of view, a good agreement has been achieved – but that is for the reader of this paper to decide

The question arises as to what extent a change in tool geometry influences the cutting process. The result is shown in Figure 12.

The kinematic conditions are similar to the results already discussed and presented in Figure 5. Material flows into the "funnel" and cannot continue due to the singularity (C3). Only when the singularity opens can the material flow continue (this opening always occurs in the direction of lowest resistance). Due to the "harden BUE," in this case, the singularity opens upward, and that is indicated by the yellow and by the red triangle in Figure 12. This movement results – according to the Newton's axiom – in additional body forces (see equation (7) $a(t)$).

In addition, the moving particle of the BUE could be demonstrated, and this is the result of the dynamic opening of the "funnel."

Figures 12

The cutting conditions under BUE with a negative rake angle creating grid deformation and based on the given strain rate and corresponding stress situation

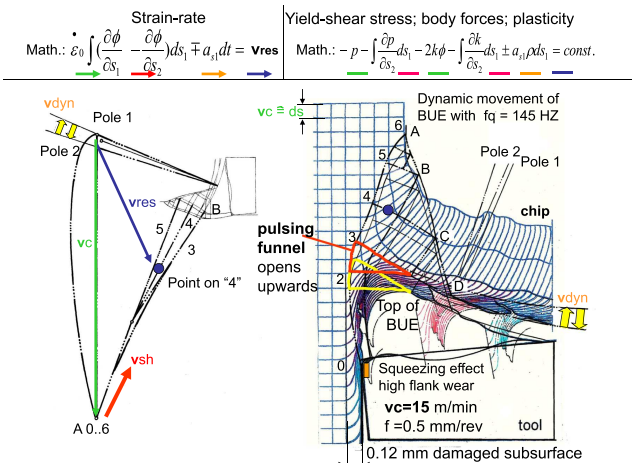
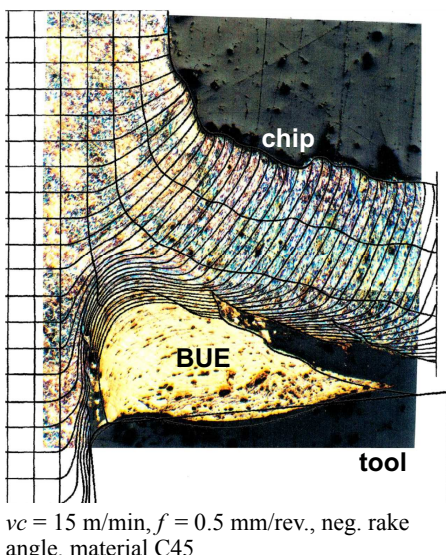


Figure 13

Evidence between practical and theoretical result



The frequency of the dynamic breakdown of the BUE-tip is about $f_q = 145$ HZ, and the movement of the material from the top of the BUE is indicated in color in Figure 12.

The different tool geometry of $\alpha = -6^\circ$ leads to less plastic deformation in the workpiece subsurface (influenced depth = 0.12 mm instead of 0.22 during cutting with a positive rake angle). But the bending of the chip radius is greater.

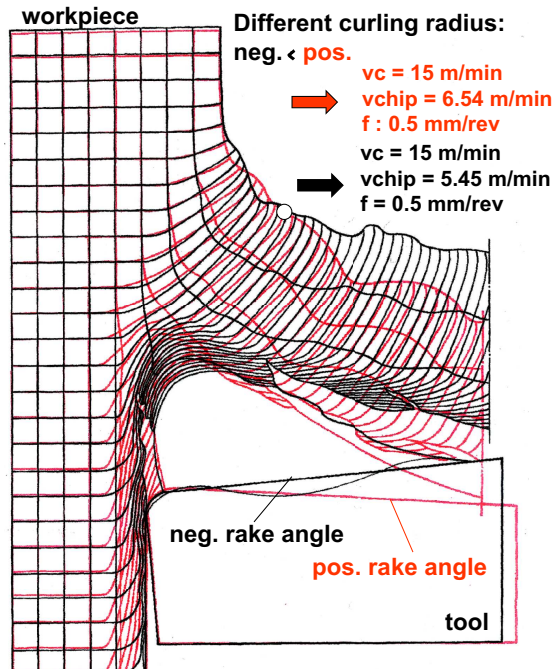
The comparison between the practical and theoretically developed results is given in Figure 13. Again, a high correlation could be achieved.

The result from a positive rake angle ($\alpha = +6^\circ$) compared with the result of a negative rake angle ($\alpha = -6^\circ$) is demonstrated in Figure 14.

From this figure, it can be obtained that the chip velocity for the positive rake angle v_{chip} has a value of 6.54 m/min, and for a

Figure 14

The different grid deformation structures under cutting with different tool geometries with positive and negative rake angles



negative rake angle, v_{chip} will be 5.45 m/min. But more important is the curling radius. The curling radius of the positive rake angle is much higher than the curling radius of the negative rake angle. This leads automatically to a larger opening angle, which in turn leads to a higher rotation of the entire deformation area.

The squeezing effect between the tool and the subsurface delivers different hardness respective residual stresses in the workpiece subsurface. The damaged zone in the subsurface with a positive rake angle is nearly twice as high. This leads to different values of flank wear.

The frequency of the dynamic breakdown of the BUE-top is nearly the same ($f_q = 145$ HZ).

3.6. Temperatures during the cutting process

The procedure of equating temperatures is an approximation for a very complex and difficult situation.

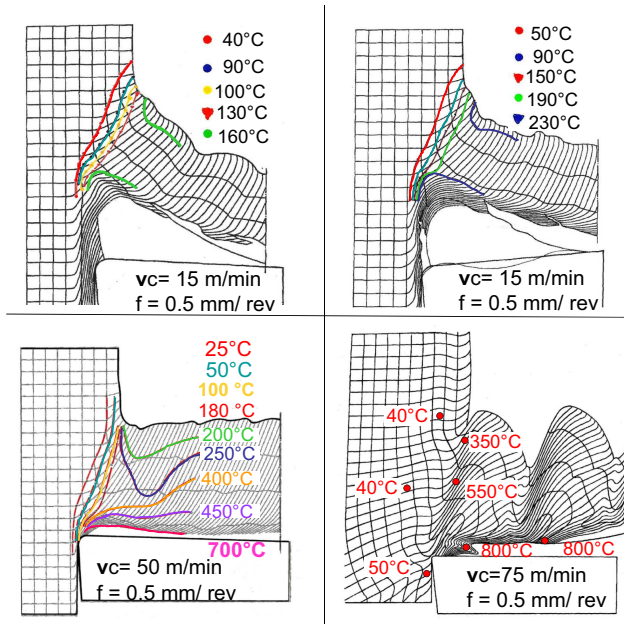
There exists no formula for describing the temperatures in relation to stress, strain, density, mechanical equivalent of heat, and the resulting deformation "ds" during processing – that's a fact. But all parameters depend on temperatures. Therefore, in this paper, an alternative approach for an appropriate thermodynamic analysis will be presented.

In Section 3.2, it was shown that the strain rate and corresponding yield shear stress have an interdependent relationship during plasticity under friction conditions. This fact leads to the opportunity to create the temperatures on material properties and metallurgical behavior without any assumptions of heat transfer, etc.

In Figure 2, the average yield shear stress k_f is given versus natural strain as well as versus temperatures T for the material C45. Each deformation results in a temperature change (in situ). With higher temperature, the average yield shear stress will decrease, but

Figure 15

Demonstrate the temperature values (lines and points) for different cutting conditions in the plastic deformation zone (in situ)



deformation will increase. This relationship will be influenced by some nonlinearities “Blue brittleness” or “ α - γ ” transformation.

As long as we know the natural strain development during the cutting operation (given by do/ds), it will be possible to determine the corresponding temperature. (An example is given in Figure 2 in green color. If we get a deformation $do/ds = 5$, we get a temperature of 600°C. Connecting all deformations of “ $\varphi = 5$,” then a “line” with constant temperatures can be estimated in situ.)

Thus, step by step, the thermal distribution can be developed in the physical plane, even if some nonlinearities exist.

At the boundary line “A” the temperature will be 25°C and the yield shear stress $k_f = 550 \text{ N/mm}^2$ (see left-hand side of Figure 2). With increasing deformation, the temperatures will increase.

All the other temperatures depend on the plastic deformation process ($\varphi = do/ds$) during cutting. The change from α to γ -Fe starts at a temperature of 723°C, and that is the temperature in the BUL. Furthermore, during cutting under “self-blocking,” the temperatures are nearly 800°C in the contacting area (see Figure 15).

But if we wait long enough, all temperatures disappear and the total material has room temperature. In other words, the created temperatures are a function of time and space.

4. Conclusion

Nearly all previous theoretical or practically orientated results of the metal cutting process create more questions than they give answers. The models try to solve the metal plastic material flow by force or stress simulation, without regarding the existing physical relationships at the interface between material and tool such as BUE, BUL, or chip self-blockade. These complex contact conditions are based on the intercrystallite metal structure, and the material can

flow only on special gliding lines, creating a complex deformation field. This deformation field collided with the stress field from metal plasticity and created a singularity. This singularity must open periodically, and this effect is responsible for the dynamic cutting process.

– **Mathematical development:** Based on tensor mathematics, the relevant equations to describe the stress as well as the strain-rate situation could be developed, taking into account real existing material behavior. The plastic deformation depends on yield shear stress k as well as on the hydrostatic pressure p . It was shown that the hydrostatic pressure p in particular determines the first deformation line.

– **Contact and Friction conditions:** Our previous thinking and equating the contact behavior is based on a modification of the Coulomb friction law. But during plastic deformation, the situation is quite different. At the interface between tool and material, a “dead zone” will be created. The position of this “dead zone” is influenced by the kinematics as well as the tool geometry. With low cutting velocity, BUE will be created, and with higher vc , the BUE changes into BUL, as a result of the 700°C temperature in the contacting area. With increasing vc , the chip velocity “ v_{chip} ” is very small, and a chip blockade takes place, creating a segmented chip. The big problem is to visualize these complex phenomena. But this was done and presented in this paper.

– **Material behavior:** As a result of the intercrystallite structure, the material deforms only on maximum shear lines (τ_{\max}). The ductility of the material is determined in particular by the hydrostatic pressure p . There is only one disadvantage: the hydrostatic pressure p and the yield shear stress are not constant but will change due to self-hardening or temperature effects, as documented in this paper.

– **Temperatures:** All parameters involved in this process depend on temperatures. The main influencing parameter is the cutting velocity vc . Furthermore, the temperatures vary in time and position. Under these circumstances, the equating of temperatures is a countless attempt for developing the real existing values. That is the reason why, in this paper, an alternative approach has been developed. Based on measured material behavior (see Figure 2), the stress values and the strain values depend on temperatures. As long as we know the correct deformation or if you like strain values, the determination of the temperature (in situ) can be estimated.

– **Evident between practical and theoretical grid deformation:** For different cutting velocities vc from 15...50...75 m/min, the theoretical grid deformation structure, including relevant contact and friction conditions, could be developed and is presented in this paper. In addition, some own quick-stop tests were used to ensure that the material specification, the feed, the tool specification, and the machinery will be identical (these “quick-stops” were generated with the help of a newly developed setup). Great importance was attached to the selection of explosive cartridges (ammunition). The resulting cross-sections could be compared with the theoretically developed deformation. In all cases, a good agreement between the practical and theoretical results could be achieved.

That leads to the final conclusion - we can develop the mathematical algorithm for creating a digital machine process with a high degree of conformity between experimental and calculated result before processing.

Nomenclature

a	acceleration
A1, A2	lines of constant stress and strain
BCD	lines of constant stress and strain
ds	deformation
g	gravitational acceleration
k	shear stress in Mohr's circle
k_f	yield shear stress
m	mass
p	hydrostatic pressure in Mohr's circle
$s1; s2$	orthogonal lines of yield shear stress
T	temperature
t	time
vc	cutting speed
v_{chip}	chip velocity
v_{dyn}	vector for dynamic velocity
$v_{sh.}$	speed vector with self-hardening
v_{res}	resultant velocity
V	volume
$\dot{\epsilon}$	strain rate
ϕ	rotation angle in Mohr's circle
$\dot{\gamma}$	shear strain-rate coordinate in Mohr's circle
φ	natural strain
μ	coefficient of friction
μ_{ext}	coefficient of friction chip tool
μ_{int}	coefficient of friction inside material
ρ	density
σ	normal stress
$\sigma_m = p$	hydrostatic stress
τ	shear strength

Ethical Statement

This study does not contain any studies with human or animal subjects performed by the author.

Conflicts of Interest

The author declares that he has no conflicts of interest to this work.

Data Availability Statement

Data are available from the corresponding author upon reasonable request.

Author Contribution Statement

Wolfgang Lortz: Conceptualization, Methodology, Software, Validation, Formal analysis, Investigation, Resources, Data curation, Writing – original draft, Writing – review & editing, Visualization, Supervision, Project administration.

References

- [1] Merchant, M.E. (1945). Mechanics of the metal cutting process, orthogonal cutting and a type II chip. *Applied Physics*, 16(5), 267–275. <https://doi.org/10.1063/1.1707586>
- [2] Shaw, M.C. (2005). *Metal cutting principles* (2nd ed.).
- [3] Schulze, V., Michna, J., Zanger, F., & Pabst, R. (2011). Modeling the process-induced modifications of the microstructure of work piece surface zones in cutting processes. *Advanced Materials Research*, 223, 69–72. <https://doi.org/10.4028/www.scientific.net/AMR.223.371>
- [4] Zhang, C., & Choi, H. (2021). Study of Segmented Chip Formation in cutting of high-strength lightweight alloys. *International Journal of Advanced Manufacturing Technology*, 112(9–10), 2755–2771. <https://doi.org/10.1007/s00170-020-06057-4>
- [5] Hardt, M., & Bergs, T. (2021). The three-dimensional numerical modeling of face turning using the Coupled-Eulerian-Lagrangian formulation. *Procedia CIRP*, 102, 162–167. <https://doi.org/10.1016/j.procir.2021.09.028>
- [6] Arriola, I., Whitenton, J., Heigel, E., & Arrazola, P.J. (2011). Relationship between machinability index and in-process parameters during orthogonal cutting of steels. *CIRP Annals Manufacturing Technology*, 60(1), 93–96. <https://doi.org/10.1016/j.cirp.2011.03.082>
- [7] Plogmeyer, M., Gonzalez, G., Schulze, V., & Bräuer, G. (2020). Development of thin-film based sensors for temperature and tool wear monitoring during machining. *TM Technisches Messen*, 87(12), 768–776. <https://doi.org/10.1515/teme-2020-0058>
- [8] Lortz, W., & Pavel, R. (2021). Advanced modeling of drilling-realistic process mechanics leading to helical chip formation. In *International Manufacturing Science and Engineering Conference*, 85079, V002T06A028.
- [9] Bergs, T., Biermann, D., Erkorkmaz, K., & M'Saoubi, R. (2023). Digital twins for cutting processes. *CIRP Annals Manufacturing Technology*, 72, 541–567. <https://doi.org/10.1016/j.cirp.2023.05.006>
- [10] Meurer, M., Tekkaya, B., Augspurger, T., Pullen, T., Schraknepper, D., Bergs, T., & Munstermann, S. (2020). Cutting force based surface integrity soft-sensor when hard machining AISI 4140. *TM Technisches Messen*, 87(11), 683–693. <https://doi.org/10.1515/teme-2020-0050>
- [11] Shan, C., Zhang, M., Zhang, S., & Dang, J. (2020). Prediction of machining-induced residual stress in Orth. *Cutting of Ti-6Al4V. The International Journal of Advanced Manufacturing Technology*, 107(5–6), 2375–2385. <https://doi.org/10.1007/s00170-020-05181-5>
- [12] Careri, F., Imbrogno, S., Umbrello, D., Outeiro, J.C., & Batista, A.C. (2021). A residual stress prediction of machining IN718 produced by direct energy deposition. *Procedia CIRP*, 102, 13–18. <https://doi.org/10.1016/j.procir.2021.09.003>
- [13] Wegert, R., Guski, V., Möhring, H.C., & Schmauder, S. (2020). Temperature monitoring in the subsurface during single lip deep hole drilling. *TM Technisches Messen*, 87(12), 757–767. <https://doi.org/10.1515/teme-2020-0055>
- [14] Moritz, J., Seidel, A., Kopper, M., Bretschneider, J., Gumpinger, J., & Finaske, T. (2020). Hybrid manufacturing of titanium Ti-6Al-4V combining laser metal deposition and cryogenic milling. *International Journal of Advanced Manufacturing Technology*, 112(9–10), 2773–2787. <https://doi.org/10.1007/s00170-020-06058-3>

Manufacturing Technology, 107, 2995–3009. <https://doi.org/10.1007/s00170-020-05212-1>

[15] Saelzer, J., Berger, S., Iovkov, I., Zabel, A., & Biermann, D. (2020). In-situ measurement of rake face temperatures in orthogonal cutting. *CIRP Annals of Manufacturing Technology*, 69, 61–64. <https://doi.org/10.1016/j.cirp.2020.04.021>

[16] Öznel, T., Biermann, D., Enomoto, T., & Mativenga, P. (2021). Structured and textured cutting tool surfaces for machining applications. *CIRP Annals – Manufacturing Technology*, 70, 495–518. <https://doi.org/10.1016/j.cirp.2021.05.006>

[17] Samy, E.O., & Ayman, M.A. (2011). Mathematical modeling experimental approach of the friction on the tool-chip interface of multicoated carbide turning inserts. *International Scholarly and Scientific Research & Innovation*, 5(3), 1–24.

[18] Lin, H.M., Liao, Y.S., & Wie, C.C. (2008). Wear behavior in turning high hardness alloy steel by CBN tool. *Wear*, 264, 679–684. <https://doi.org/10.1016/j.wear.2007.06.006>

[19] Puls, H., Klocke, F., & Lung, D. (2014). Experimental investigation on friction under metal cutting conditions. *Wear*, 310(1–2), 63–71. <https://doi.org/10.1016/j.wear.2013.12.020>

[20] Smolenicki, D., Boos, J., Kuster, F., Roefolds, H., & Wyen, C.F. (2014). In-process measurement of friction coefficient in orthogonal cutting. *CIRP Annals Manufacturing Technology*, 60(1), 97–100. <https://doi.org/10.1016/j.cirp.2014.03.083>

How to Cite: Lortz, W. (2025). Metal Cutting Data Integration with Different Contact and Friction Conditions, Kinematics, Tool Geometry, and Temperatures. *Archives of Advanced Engineering Science*. <https://doi.org/10.47852/bonviewAAES52027300>